CHIN. PHYS. LETT. Vol. 38, No. 4 (2021) 047201

Non-Monotonic Evolution of Carrier Density and Mobility under Thermal Cycling Treatments in Dirac Semimetal Cd_3As_2 Microbelts

Zheng Chen(陈正)[1,2†], Min Wu(武敏)[1,2†], Yequn Liu(刘叶群)[3], Wenshuai Gao(高文帅)[4], Yuyan Han(韩玉岩)[1], Jianhui Zhou(周建辉)[1*], Wei Ning(宁伟)[1*], and Mingliang Tian(田明亮)[1,4]

[1]*Anhui Province Key Laboratory of Condensed Matter Physics at Extreme Conditions, High Magnetic Field Laboratory, Chinese Academy of Sciences, Hefei 230031, China*

[2]*Department of Physics, University of Science and Technology of China, Hefei 230026, China*

[3]*Analytical Instrumentation Center, State Key Laboratory of Coal Conversion, Institute of Coal Chemistry, Chinese Academy of Sciences, Taiyuan 030001, China*

[4]*Department of Physics, School of Physics and Materials Science, Anhui University, Hefei 230601, China*

(Received 18 December 2020; accepted 9 February 2021; published online 6 April 2021)

Tunable carrier density plays a key role in the investigation of novel transport properties in three-dimensional topological semimetals. We demonstrate that the carrier density, as well as the mobility, of Dirac semimetal Cd_3As_2 nanoplates can be effectively tuned via *in situ* thermal treatment at 350 K for one hour, resulting in non-monotonic evolution by virtue of the thermal cycling treatments. The upward shift of Fermi level relative to the Dirac nodes blurs the surface Fermi-arc states, accompanied by an anomalous phase shift in the oscillations of bulk states, due to a change in the topology of the electrons. Meanwhile, the oscillation peaks of bulk longitudinal magnetoresistivity shift at high fields, due to their coupling to the oscillations of the surface Fermi-arc states. Our work provides a thermal control mechanism for the manipulation of quantum states in Dirac semimetal Cd_3As_2 at high temperatures, via their carrier density.

DOI: 10.1088/0256-307X/38/4/047201

Since the discovery of three-dimensional (3D) Dirac semimetal Cd_3As_2,[1–3] a number of unusual transport properties have been observed experimentally, such as ultra-high carrier mobility,[4–6] negative longitudinal magnetoresistivity (LMR),[7–9] and quantum oscillations of surface Fermi-arc states.[10,11] Experimentally, one of the main obstacles to revealing exotic quantum phenomena is the problem of modulating the carrier concentrations in 3D bulk states. Conventional gating technologies, such as the back gate[12–15] and the electrolyte gate,[16–19] can achieve effective modulation of carriers for thin samples with very low carrier densities. However, a 3D Dirac semimetal is hard to tune effectively by means of these conventional gating technologies, for several reasons. Firstly, 3D Dirac semimetals usually have a conducting bulk state with high carrier concentrations, greatly reducing the efficiency of gating. Secondly, the Dirac nodes of Cd_3As_2 can only be well maintained in microbelts thicker than 60 nm,[1,20] below which the Dirac node will open a gap, due to the quantum confinement effect.[1,21,22] Therefore, the discovery of a feasible method of effectively tuning the carrier density in Dirac semimetal Cd_3As_2 microbelts is highly desirable.

In this Letter, we demonstrate that the carrier concentrations evolve non-monotonically when undergoing a thermal cycling treatment (TCT) whereby samples are repeatedly annealed at 350 K for one hour. As the cycling treatment goes on, both the carrier density and mobility exhibit an anomalous evolution. A temporarily upward-shifted Fermi energy, originating from the fluctuation of carrier concentrations, blurs the surface Fermi-arc states, and changes the Fermi surface topology, resulting in an anomalous phase shift of the bulk quantum oscillations. Our results provide an alternative approach to modulating the carrier concentrations and transport properties of Cd_3As_2 microbelts.

The crystal structure of Cd_3As_2 can be regarded as a distorted anti-fluorite structure with exactly ordered 1/4 Cd vacancies, arranged helically along the [001] direction in the ideal lattice.[23] In this tetragonal structure, the arsenic atoms form a closed-packed cubic shape, and the cadmium atoms are four-coordinated by the arsenic, as shown in Fig. 1(a). In our experiments, the Cd_3As_2 microbelts were grown using the chemical vapor deposition (CVD) method. The scan-

Supported by the National Key Research and Development Program of China (Grant No. 2016YFA0401003), and the National Natural Science Foundation of China (Grant Nos. 11804340, 11774353, U19A2093, and U1732274), and the CAS/SAFEA International Partnership Program for Creative Research Teams of China.

†Those authors contributed equally to this work.

*Corresponding author. Email: jhzhou@hmfl.ac.cn; ningwei@hmfl.ac.cn

© 2021 Chinese Physical Society and IOP Publishing Ltd

ning electron microscopy (SEM) image in Fig. 1(b) shows that the length of microbelts can measure as much as 100 μm, far longer than those reported in previous works (∼10 μm).[24–26] The characterization of Cd_3As_2 microbelts via high-resolution transmission electron microscopy (HR-TEM) is illustrated in Fig. 1(c).

The HR-TEM and the selected area electron diffraction (SAED) pattern in Fig. 1(d) demonstrate a [221] zone axis, indicating that the naturally grown surface is the (112) plane. The Cd_3As_2 microbelts were then fabricated into standard Hall-bar configurations, and coated with Ti/Au electrodes (10/120 nm) by means of standard electron-beam lithography (EBL) and lift-off techniques. We selected thick samples (>70 nm) to prevent the gap opening of bulk states, and to ensure the topologically semimetallic nature of the Dirac fermions in Cd_3As_2 microbelts. A typical Hall-bar device (sample 1), with a thickness of about 90 nm is presented in the inset of Fig. 1(a). To avoid contamination or oxidation at the surface, the Hall-bar devices were covered with poly-methyl methacrylate layers prior to transport measurement.

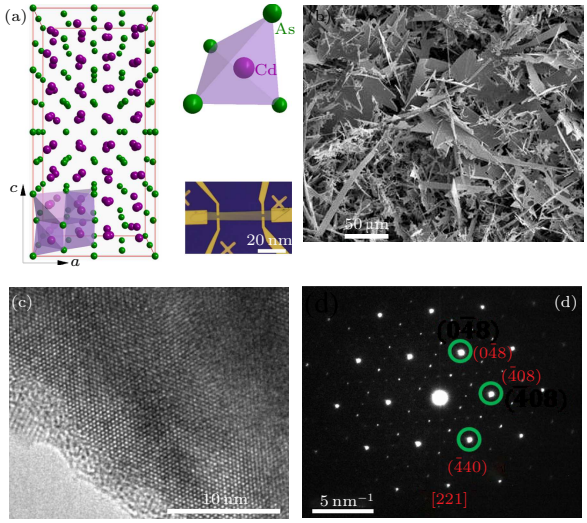

Fig. 1. (a) Crystalline structure of Cd_3As_2, with a body-centered tetragonal structure. Upper inset: the basic structure of Cd_3As_2. Lower inset: optical microscope image of sample 1, with a thickness of about 90 nm. (b) SEM image of CVD-grown Cd_3As_2 nanoplates. Scale bar: 50 μm. (c) HR-TEM image of Cd_3As_2 nanoplate. Scale bar: 10 nm. (d) Corresponding SAED pattern.

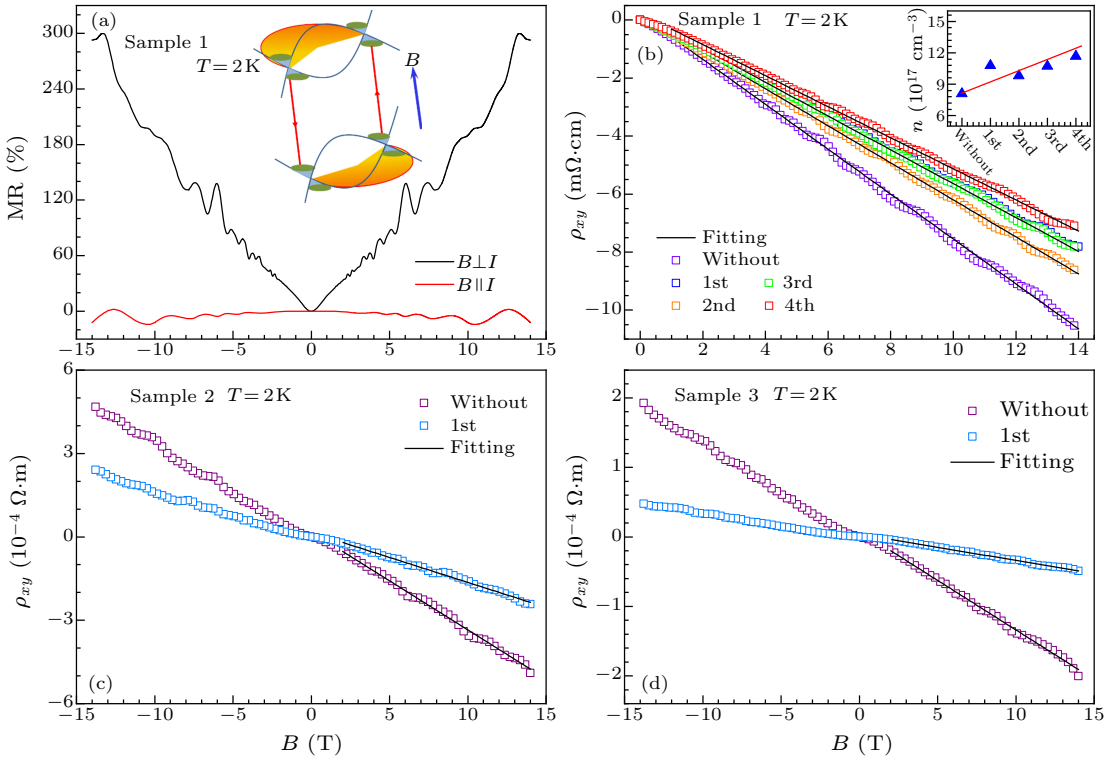

Fig. 2. (a) Multi-periodic (black) and single periodic (red) SdH oscillations, observed in sample 1 at $T = 2$ K with $B \perp I$ and $B \parallel I$, respectively. Inset: an illustration of Weyl magnetic orbits. (b) Hall resistivity, measured without (marked "without") and with (marked 1st, 2nd, 3rd and 4th) TCTs in sample 1. Inset: the corresponding carrier density for each measurement. (c) and (d) Hall resistivity, measured without and with 1st TCT, in samples 2 and 3, whose thicknesses measure approximately 100 nm and 120 nm, respectively.

Figure 2(a) shows the LMR of sample 1 at 2 K for the magnetic field B, parallel ($\theta = 90°$) and perpendicular ($\theta = 0°$) to the electric current, I. For $\theta = 90°$, only single-periodic Shubnikov-de Haas (SdH) oscillations are revealed, and superimposed on the negative LMR. The negative LMR in Cd_3As_2 could be attributed to a chiral anomaly.[7–9] For $\theta = 0°$, the large positive LMR exhibits multi-periodic oscillation

patterns, which may originate from the unusual Weyl orbits connecting the Fermi-arcs on the opposite surfaces via bulk chiral modes.[27] These multi-periodic oscillations were also observed in samples 2 and 3 (see Supplementary Information). If we heat the sample *in situ* to 350 K, maintaining this temperature for one hour (at helium gas ambient, and at a pressure of less than 1 Torr), followed by cooling down to 2 K, the Hall coefficient $R_{\rm H} = 1/ne$ (negative) increases correspondingly. Repeating this process (TCT) four times [marked 1st, 2nd, 3rd and 4th in Fig. 2(b)], the Hall coefficient $R_{\rm H}$ increases accordingly, indicating an enhancement of the carrier density. This can also be seen in the inset of Fig. 2(b), where the carrier density changes from $8.1 \times 10^{17}\,{\rm cm}^{-3}$ (without TCT) to $1.17 \times 10^{18}\,{\rm cm}^{-3}$ after the four consecutive TCTs. For a band with Dirac dispersion, $E_{\rm F} = \hbar v_{\rm F} \left(3\pi^2 n\right)^{1/3}$, where $\hbar$ denotes Planck's constant, and $v_{\rm F}$ is the Fermi velocity, the increase of n in sample 1 indicates that $E_{\rm F}$ shifts upward, away from the Dirac points. This upward shift in $E_{\rm F}$ allows us to study the magneto-transport properties of the Fermi-arc surface states for different Fermi levels. The Hall resistivity measurements in samples 2 and 3 also exhibit an evident enhancement of the carrier density after the first TCT, as shown in Figs. 2(c) and 2(d).

Table 1. Sample thickness, Fermi energy, carrier mobility, density, bulk frequency, and surface frequency for the three samples, without TCT.

Sample	1	2	3
t (nm)	90	100	120
$E_{\rm F}$ (meV)	76	46	61
$\mu\,(10^5\,{\rm cm}^2{\cdot}{\rm V}^{-1}{\cdot}{\rm s}^{-1})$	1.3	1.56	2.5
$n\,(10^{17}\,{\rm cm}^{-3})$	8.1	1.8	4.3
$F_{\rm bulk}$ (T)	30	18	29
$F_{\rm surface}$ (T)	62	32	66

In order to gain further insights into the impact of TCT on carrier density, we performed additional measurements on samples 2 and 3, as shown in Fig. 3. It is worth pointing out that the carrier density in both samples (without TCT) is much lower than that in 1, as shown in Table 1 (the detailed extraction of carrier mobility is presented in the Supplementary Information). As shown in Fig. 3(a), the carrier density in sample 2 increases sharply after the first TCT, and then becomes saturated, forming a plateau. After the first five consecutive TCTs, the carrier density begins to gradually decrease, and ultimately tends to be saturated again. In general, annealing largely reduces defects in materials, and strongly enhances the transport lifetime $\tau_{\rm tr}$.[28,29] On the basis of the mobility of 3D Dirac fermions, $\mu = ev_{\rm F}\tau_{\rm tr}/\hbar k_{\rm F}$ with $k_{\rm F}$ being the Fermi wave vector, the carrier mobility should increase. However, as shown in Fig. 3(a), the carrier mobility exhibits an anomalous behavior, but with an opposite tendency, as compared to the carrier density after the TCTs. Similar behaviors, in terms of both carrier density and mobility, were also observed in sample 3, as depicted in Fig. 3(b).

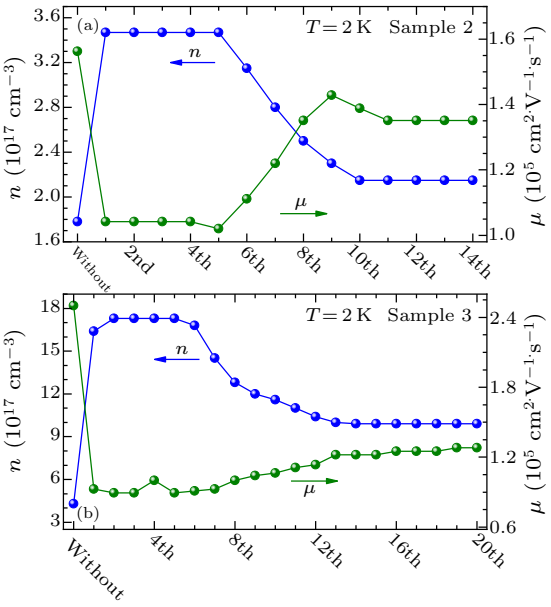

Fig. 3. Anomalous evolution of carrier density and mobility. (a) The TCT-induced evolution of carrier density and mobility in sample 2. These two effects exhibit an opposite tendency with TCTs. Similar behavior is also evident in sample 3 in (b).

As mentioned above, without the TCT, the LMR of sample 1 exhibits multi-periodic oscillation patterns for $\theta = 0°$ at 2 K. Tilting the field away from the direction $\theta = 0°$ causes the multi-periodic oscillation patterns to gradually disappear, as shown in Fig. 4(a). Above $\theta = 56°$, only single oscillation patterns are present, and the oscillation frequency remains unchanged (grey arrows), indicating the presence of an isotropic Fermi surface in the Cd_3As_2 microbelts. As noted in our previous study,[11] the extra oscillation patterns near $\theta = 0°$ at high field region may originate from the 2D oscillations of Fermi-arc states on the opposite surfaces, mediated by the bulk chiral modes. These 2D surface oscillation patterns can be confirmed based on the angular-dependent LMR oscillations. In Fig. 4(b), the oscillation patterns with kinks or peaks (the black dashed lines) indeed exhibit a 2D character. Note that, in Fig. 4(a), the LMR oscillation peaks from bulk states are shifted below $\theta = 47°$ (deviated from the grey arrows), as indicated by the red dashed curves. Generally, the quantum oscillations of 2D surface states at high fields are superimposed on the 3D bulk states without shifting the oscillation peaks from the bulk.[11] This is possibly due to the strong coupling between the surface Fermi-arcs and the bulk states, which shifts the bulk oscillations.

To illustrate the evolution of Fermi-arc surface states with respect to the bulk Fermi energy, we

present detailed oscillation patterns for sample 1 at 2 K and $\theta = 0°$ both without and with TCTs, in Fig. 4(c). Firstly, the confirmed surface-state oscillations become blurred after the TCTs, revealing a weak coupling between the surface and the bulk states. Secondly, the peak spacing of the surface-state oscillations becomes narrow, demonstrating that the oscillation frequency of surface Fermi-arcs increases with an upward shift in Fermi energy, as marked by the red arrows in Fig. 4(c). Theoretically, the oscillation frequency of the Weyl orbits, F_s is proportional to the Fermi energy, E_F, $F_s = E_F k_0/(e\pi v_F)$,[27] where k_0 is the length of the Fermi-arc states ($\sim$0.1 Å^{-1}).[5,27] Here, $k_0/(k_F^2 L)$ is the ratio of the surface to the bulk states, where L denotes the thickness of the Dirac semimetal microbelt between two opposite surfaces. As the Fermi energy shifts upward, relative to the Dirac nodes, the effective length of the Fermi-arc state shortens, and the ratio of the surface to the bulk states decreases, such that F_s increases. Our observations are, without ambiguity, qualitatively consistent with previous theoretical works.

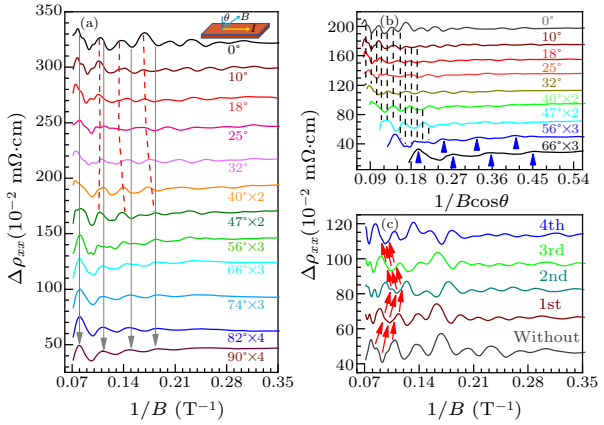

Fig. 4. Evolution of surface Fermi-arc states in sample 1. (a) Angular-dependence of oscillation components of LMR $\Delta\rho_{xx}$ without TCT, at $T = 2$ K. (b) Oscillation components $\Delta\rho_{xx}$ versus $1/B\cos\theta$ at various titled angles, without TCT. Both 2D oscillations from the surface Fermi-arcs (black dashed lines) and 3D bulk oscillations (blue arrows) are revealed. (c) Plot of $\Delta\rho_{xx}$ versus $1/B$ for each measurement, without and with TCTs, at $T = 2$ K, $\theta = 0°$. The red arrows indicate the evolution of surface Fermi-arc states.

The quantum oscillations at different Fermi energies can also help us to identify the Fermi surface topology. Figure 5(a) shows the oscillation components of LMR $\Delta\rho_{xx}$ versus $1/B$ with $B \parallel I(\theta = 90°)$ for each measurement of sample 1 at $T = 2$ K. both without and with TCTs. We present the corresponding fast Fourier transformation (FFT) spectra for each measurement to obtain the k_F in Fig. 5(b). The oscillation frequency increases noticeably, from about 30 T (without TCT) to 40 T after four consecutive TCTs, as indicated by the red arrows. In accordance with the Onsager relationship, $F(T) = \frac{\hbar}{2\pi e} A_F$ with $A_F = \pi k_F^2$ for the maximal cross-sectional area of Fermi surface, the magnitude of k_F changes correspondingly, from 3.0×10^{-2} Å^{-1} to 3.5×10^{-2} Å^{-1}. We extract the phase factor, φ via Landau level (LL) fan diagrams for each measurement in sample 1, in which we assign the oscillation peaks to the integer LL indices [Fig. 5(c)].[30] The phase factor deduced from the Lifshitz–Onsager relation, $\frac{\hbar}{eB} A_F = 2\pi(n + \varphi)$,[31,32] is shown in the inset of Fig. 5(c). It is evident that the phase factor changes monotonously from -0.18 to -0.50, approaching $-5/8$ for 3D electron gases with a parabolic dispersion. Such a phase shift reveals a clear change of topology of the Fermi surface, from a topologically nontrivial band (linear dispersion) to a trivial band structure (parabolic dispersion) in line with the upward shift in Fermi energy. The behavior of quantum oscillations with respect to Fermi energy can be qualitatively understood by means of an effective model based on *ab initio* calculations.[1,30] In addition, after the fourth TCT, the observed negative LMR is largely suppressed, which we ascribe to the Fermi energy possibly approaching the Lifshitz transition point (a more detailed discussion is presented in the Supplementary Information).

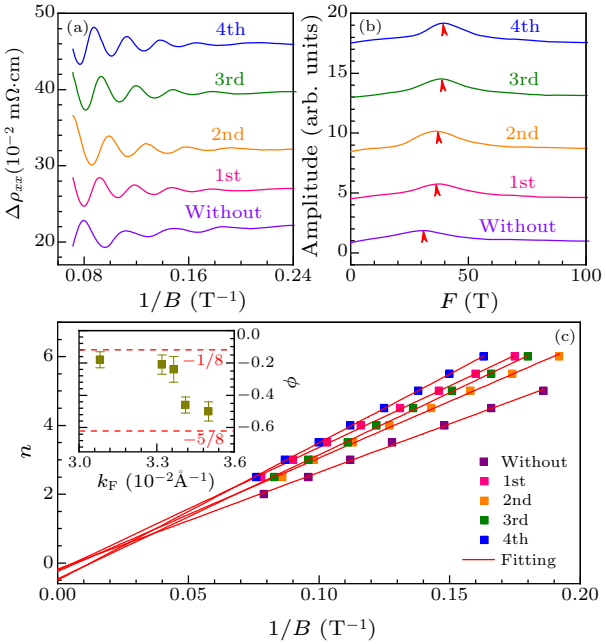

Fig. 5. The anomalous phase shift of bulk quantum oscillations in sample 1. (a) Oscillation amplitudes $\Delta\rho_{xx}$ versus $1/B$ for each measurement, without and with TCTs, in the presence of parallel electromagnetic fields at $T = 2$ K. (b) The corresponding FFT spectra. (c) The Landau level index n versus $1/B$, for each measurement. Inset: phase factor changes from -0.18 to -0.5 with an increase in the Fermi wave vectors.

Finally, we briefly discuss the possible mechanisms for the anomalous evolution of carrier density and mobility induced by the TCT in Cd_3As_2 microbelts. The

evolution of resistivity in Cd_3As_2 single crystals at room temperature has been reported before, and some mechanisms, such as surface oxidation or degradation, have been suggested.[5] In fact, surface oxidation is unlikely in our samples, since the surfaces are coated with poly-methyl methacrylate layers during throughout the transport measurements, and the TCTs are performed *in situ* in helium gas ambient conditions. The structural phase transition induced by TCT can also be ruled out, as the lowest transition temperature in Cd_3As_2 (about 220℃)[33] is far higher than the maximal temperature in our experiments (∼75 ℃). A possible mechanism may be related to the annealing, which affects the cadmium vacancies,[34,35] and creates charge puddles,[36] leading to a dramatic fluctuation in the carrier density of the Cd_3As_2 crystals. However, the carrier densities of crystals decreased consecutively after annealing at room temperature in previous experiments,[34−36] which contrasts strongly with our results for Cd_3As_2 microbelts, as given in Fig. 3. The anomalous behavior of the carrier density may be ascribed to nonequilibrium dynamics occurring during thermal treatment.[37]

In summary, we have found that non-monotonic behavior in relation to carrier density can be induced in Cd_3As_2 microbelts via thermal cycling treatments. A temporary upward shift of the bulk Fermi level suppresses the surface Fermi-arc states, leading to an anomalous phase shift in the bulk quantum oscillations. The possible origins of the anomalous evolution of the carrier density and mobility have been discussed above. Our findings indicate that thermal-induced carrier evolution should be considered in Cd_3As_2-based thermoelectric devices.

References

[1] Wang Z J *et al.* 2013 *Phys. Rev. B* **88** 125427
[2] Liu Z K *et al.* 2014 *Nat. Mater.* **13** 677
[3] Borisenko S *et al.* 2014 *Phys. Rev. Lett.* **113** 027603
[4] He L P *et al.* 2014 *Phys. Rev. Lett.* **113** 246402
[5] Liang T *et al.* 2015 *Nat. Mater.* **14** 280
[6] Feng J Y *et al.* 2015 *Phys. Rev. B* **92** 081306
[7] Li C Z *et al.* 2015 *Nat. Commun.* **6** 10137
[8] Li H *et al.* 2016 *Nat. Commun.* **7** 10301
[9] Wu M *et al.* 2018 *Phys. Rev. B* **98** 161110
[10] Moll P J W *et al.* 2016 *Nature* **535** 266
[11] Zheng G L *et al.* 2017 *Phys. Rev. B* **96** 121407
[12] Novoselov K S *et al.* 2004 *Science* **306** 666
[13] Zhang Y B, Tan Y W, Stormer H L and Kim P 2005 *Nature* **438** 201
[14] Chen J *et al.* 2011 *Phys. Rev. B* **83** 241304
[15] Yoshimi R *et al.* 2015 *Nat. Commun.* **6** 6627
[16] Ye J T *et al.* 2010 *Nat. Mater.* **9** 125
[17] Kong D *et al.* 2011 *Nat. Nanotechnol.* **6** 705
[18] Yuan H *et al.* 2011 *Nano Lett.* **11** 2601
[19] Shimizu S *et al.* 2012 *Phys. Rev. B* **86** 045319
[20] Cheng P H *et al.* 2016 *New J. Phys.* **18** 083003
[21] Xiao X *et al.* 2015 *Sci. Rep.* **5** 7898
[22] Pan H, Wu M M, Liu Y and Yang S A 2015 *Sci. Rep.* **5** 14639
[23] MN A *et al.* 2014 *Inorg. Chem.* **53** 4062
[24] Li C Z *et al.* 2016 *ACS Nano* **10** 6020
[25] Zhang C *et al.* 2017 *Nat. Commun.* **8** 13741
[26] Wang Q *et al.* 2017 *Nano Lett.* **17** 834
[27] Potter A C, Kimchi I and Vishwanath A 2014 *Nat. Commun.* **5** 5161
[28] Globisch B *et al.* 2016 *AIP Adv.* **6** 125011
[29] Okuda T *et al.* 2014 *Appl. Phys. Express* **7** 085501
[30] Wang C M, Lu H Z and Shen S Q 2016 *Phys. Rev. Lett.* **117** 077201
[31] Shoenberg D 1984 *Magnetic Oscillations in Metals* (Cambridge: Cambridge University Press)
[32] Murakawa H *et al.* 2013 *Science* **342** 1490
[33] Arushanov E 1992 *Prog. Cryst. Growth Charact. Mater.* **25** 131
[34] Blom F A P and Gelten M J 1979 *Phys. Rev. B* **19** 2411
[35] EK A 1980 *Prog. Cryst. Growth Charact. Mater.* **3** 211
[36] Crassee I *et al.* 2018 *Phys. Rev. B* **97** 125204
[37] Ma J, Wei S H, Gessert T A and Chin K K 2011 *Phys. Rev. B* **83** 245207

Supplementary Information for "Non-Monotonic Evolution of Carrier Density and Mobility under Thermal Cycling Treatments in Dirac Semimetal Cd_3As_2 Microbelts"

Zheng Chen(陈正)[1,2‡], Min Wu(武敏)[1,2‡], Yequn Liu(刘叶群)[3], Wenshuai Gao(高文帅)[4], Yuyan Han(韩玉岩)[1], Jianhui Zhou(周建辉)[1,*], Wei Ning(宁伟)[1,*], and Mingliang Tian(田明亮)[1,4]

[1] *Anhui Province Key Laboratory of Condensed Matter Physics at Extreme Conditions, High Magnetic Field Laboratory, Chinese Academy of Sciences, Hefei 230031, China.*

[2] *Department of physics, University of Science and Technology of China, Hefei 230026, China.*

[3] *Analytical Instrumentation Center, State Key Laboratory of Coal Conversion, Institute of Coal Chemistry, Chinese Academy of Sciences, Taiyuan 030001, China.*

[4] *Department of Physics, School of Physics and Materials Science, Anhui University, Hefei 230601, China.*

[‡]Those authors contribute equally to this work.

[*]To whom correspondence should be addressed. E-mail: jhzhou@hmfl.ac.cn; ningwei@hmfl.ac.cn (W.N.)

1. The carrier mobility and density

For a magnetic field perpendicular to the sample plane ($\theta = 0°$), the emergence of extra quantum oscillations in sample#1 at high fields without thermal cycling treatment (TCT), as shown in Fig. 2(a) of main text and Fig. S1(a), can be attributed to the surface Fermi-arcs participating in unusual Weyl magnetic orbits [1], and have been detailedly discussed in the main text. The Fermi-arc-mediated quantum oscillations are also observed in samples #2 and #3 with $B > 6\,T$ and $B > 9\,T$, as plotted in Figs. S1(b) and S1(c), respectively.

Due to the suppression of backscattering by π Berry phase in topological semimetals with a *k*-linear dispersion, a high carrier mobility is expected. To obtain the mobility of Cd_3As_2 microbelts, we have carried out the Hall resistivity measurements at T = 2 K without TCT and the measured resistivity (ρ_{xx} and ρ_{xy}), as plotted in Figs. S1(a)-S1(c), has been converted to the conductivity (σ_{xx} and σ_{xy}), as depicted in Figs. S1(d)-S1(f). The carrier mobility can be estimated by standard Bloch-Boltzmann transport formula [2], $\mu_1 = \mu_m\sqrt{\gamma}$, where $\mu_m = \sqrt{\mu_1\mu_2} = \frac{1}{B_{max}}$ with B_{max} the field corresponding to the peak position of $\sigma_{xy}(B)$ and $\gamma = \rho_2/\rho_1$ the resistivity anisotropy. The subscripts 1 and 2 refer to the current direction along the longitudinal and transverse directions, respectively. The resistivity anisotropy γ is about 25, as studied in our previous work [3]. The carrier mobility deduced from μ_m is shown in Table 1 of main text, the obtained carrier mobility in our microbelts is comparable with previous studies of Cd_3As_2 single crystals [2].

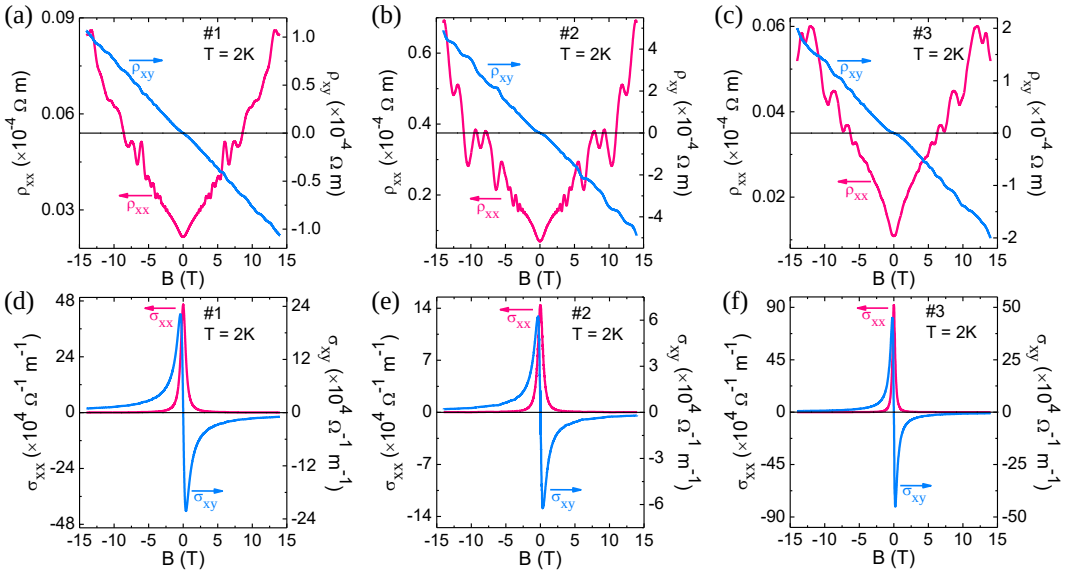

Fig. S1. (Color online) (a-c) The longitudinal magnetoresistivity and Hall resistivity for samples #1, #2 and #3 at $T = 2$ K, respectively, without the TCT. (d-f) The corresponding longitudinal magnetoconductivity and Hall conductivity.

2. Negative longitudinal magnetoresistivity and Scattering time τ_c

Another striking feature in Weyl/Dirac semimetals is the negative LMR, which is usually attributed to the chiral anomaly. While a temporarily upward-shifted Fermi level would suppress this negative LMR, due to the change of the band topology. We believe that after the fourth TCTs in sample #1, the Fermi energy is approaching the Lifshitz transition point where the single Fermi surface encloses two Dirac cones. This is well illustrated in our experiments, as we can see in Fig. S2(a), the negative LMR has been largely suppressed after four TCTs. In the picture of chiral anomaly, this can also be well identified via the intervalley scattering time τ_c of chiral charges. According to the semi-classical transport theory [4], in weak field limit, the positive conductivity induced by chiral anomaly is proportional to B^2. Indeed, this quadratic field

dependence is consistent with our experimental observations in low magnetic fields, as shown in Fig. S2(b). Theoretically, the ratio between the chiral anomaly induced conductivity increment $\delta\sigma_{xx}$ and zero field conductivity σ_0 can be written as [4]:

$$\frac{\delta\sigma_{xx}}{\sigma_0} = \frac{3}{4}\frac{e^2 v_F^2}{E_F^2 k_F^2} B^2 \frac{\tau_c}{\tau_{tr}} \qquad (1)$$

with τ_{tr} the transport lifetime. Fitting the temperature-dependent oscillation amplitudes to the Lifshitz-Kosevich formula [5,6], we can get the effective mass which changes from $0.039\, m_e$ to $0.043\, m_e$ after the four TCTs. The transport lifetime can be deduced by the relationship $\tau_{tr} = \mu\hbar k_F / e v_F$ with Fermi velocity $v_F = \hbar k_F / m^*$. Finally, we get the scattering time τ_c, which decreases from $4 \times 10^{-12}\, s$ to $1.35 \times 10^{-12}\, s$ after four TCTs. The dramatic damping of the scattering time τ_c gives another evidence that the upward shifting of the Fermi energy suppresses the chiral charge pumping in Cd_3As_2 microbelts due to the change of the band topology.

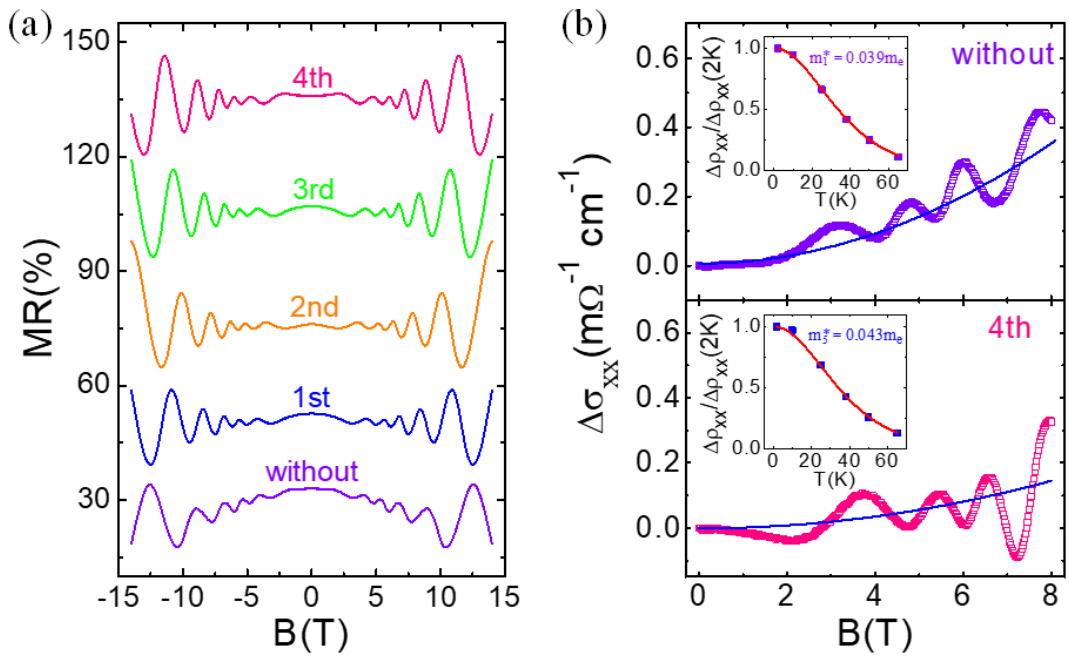

Fig. S2. (Color online) (a) The chiral anomaly induced negative LMR in parallel electromagnetic fields at $T = 2$ K for each measurement with and without the TCTs

in sample #1. (b) The positive longitudinal magnetoconductivities before and after the TCTs at $T = 2$ K. The blue curves are the fitting of the magnetoconductivity backgrounds to B^2-type function. Inset: The fittings of the temperature-dependent oscillation amplitudes to the Lifshitz-Kosevich formula generate the effective mass $0.039\ m_e$ and $0.043\ m_e$ before and after the TCTs, respectively.

Reference

[1] Potter AC, Kimchi I, Vishwanath A. Quantum oscillations from surface Fermi arcs in Weyl and Dirac semimetals. Nat Commun 2014;5:5161.

[2] Liang T, Gibson Q, Ali MN, et al. Ultrahigh mobility and giant magnetoresistance in the Dirac semimetal Cd_3As_2. Nat Mater 2015;14:280-284.

[3] Wu M, Zheng GL, Chu WW, et al. Probing the chiral anomaly by planar Hall effect in Dirac semimetal Cd_3As_2 nanoplates. Phys Rev B 2018;98:161110(R).

[4] Son DT, Spivak BZ. Chiral anomaly and classical negative magnetoresistance of Weyl metals. Phys Rev B 2013;88:104412.

[5] Shoenberg D. Magnetic Oscillations in Metals (Cambridge University Press, Cambridge, England, 1984).

[6] Murakawa H, Bahramy MS, Tokunaga M, et al. Detection of Berry's Phase in a Bulk Rashba Semiconductor. Science 2013;342:1490-1493.